Journal of Biomolecular NMR, 10 (1997) 263–272
KLUWER/ESCOM

J-Bio NMR 465

Three-dimensional structure of the Hck SH2 domain in solution

Weixing Zhang, Thomas E. Smithgall and William H. Gmeiner*

The Eppley Institute for Research in Cancer and Allied Diseases, The University of Nebraska Medical Center, Omaha, NE 68198-6805, U.S.A.

Received 8 April 1997
Accepted 28 May 1997

Keywords: Signal transduction; NOE reference; Improved pulse sequence; J-coupling; Stereospecific resonance assignment

Summary

The hematopoietic cellular kinase (Hck) is a member of the Src family of non-receptor protein-tyrosine kinases that is expressed predominantly in granulocytes, monocytes and macrophages. Recent observations suggest that Hck may be activated in HIV-infected macrophages and in chronic myelogenous leukemia cells that express Bcr-Abl. In order to increase our understanding of the structural basis for regulation of Hck activity under normal and pathological conditions, we have solved the solution structure of the uncomplexed Hck SH2 domain using NMR spectroscopy. A novel procedure that uses intraresidue H^N-H^α distances as references for converting NOE intensities into distance restraints has been described. A total of 1757 significant experimental restraints were derived from NMR spectroscopic data including 238 medium-range and 487 long-range distance restraints and 177 torsion angle restraints. These restraints were used in a simulated annealing procedure to generate 20 structures with the program DYANA. Superimposition of residues 5–104 upon the mean coordinate set yielded an average atomic rmsd values of 0.42 ± 0.08 Å for the N,C^α,C' atoms and 0.81 ± 0.08 Å for all heavy atoms. Rmsd values for those residues in the regions of ordered secondary structure were 0.27 ± 0.04 Å for the N,C^α,C' atoms and 0.73 ± 0.06 Å for all heavy atoms.

Introduction

The hematopoietic cellular kinase (Hck) is a member of the Src family of non-receptor protein-tyrosine kinases (PTKs) and is expressed predominantly in myeloid cells of the granulocytic and monocytic lineages (Holtzman et al., 1987; Klemsz et al., 1987; Quintrell et al., 1987; Ziegler et al., 1987). Hck expression is strongly induced during priming of the respiratory burst in macrophages (Boulet et al., 1992; Lichtenberg et al., 1992). In addition, Hck may help to couple the Fc receptor to respiratory burst activation (Ghazizadeh et al., 1994; Wang et al., 1994; Durden et al., 1995). Hck has also been linked to the urokinase plasminogen activator receptor, which is involved in neutrophil migration (Bohuslav et al., 1995). Localization of Hck to the secretory granules of human neutrophils suggests a role in the degranulation process as well (Möhn et al., 1995).

In addition to its role in phagocyte signal transduction, Hck has also been implicated in the pathogenesis of AIDS by virtue of its remarkable affinity for the HIV Nef protein. Nef is required for high titer replication of SIV and for induction of AIDS in rhesus monkeys (Kestler et al., 1991). Nef has no known catalytic activity and likely functions through interactions with cellular proteins involved in cellular activation and signaling. Nef has been shown to bind Hck, as well as Lyn, another member of the Src-family PTKs. Co-expression of Nef and Hck in rodent fibroblasts induces Hck activation and transformation, suggesting that Nef may activate Hck in HIV-in-

*To whom correspondence should be addressed.

Abbreviations: Hck, hematopoietic cellular kinase; SH, Src homology region; PTK, protein-tyrosine kinase; quercetin, 3,3',4',5,7-pentahydroxyflavone; AMP-PNP, β,γ-imidoadenosine-5'-triphosphate; IL-3, interleukin-3; IL-6, interleukin-6; LIF, leukemia inhibitory factor; GM-CSF, granulocyte-macrophage colony-stimulating factor; NOE, nuclear Overhauser effect; NOESY, nuclear Overhauser effect spectroscopy; HSQC, heteronuclear single-quantum coherence; WATERGATE, WATER suppression by GrAdient-Tailored Excitation; DTT, dithiothreitol; rmsd, root-mean-square deviation.

Supplementary material available: a table giving the ^1H, ^{13}C, and ^{15}N resonance assignments for the Hck SH2 domain including stereospecific resonance assignments of β-methylene protons and methyl groups of Val and Leu (6 pages) is available from the corresponding author, who agrees to provide this material on request to interested individuals for a period of at least 3 years following the date of publication.

TABLE 1
LIST OF PULSE SEQUENCES FOR STRUCTURE DETERMINATION OF THE Hck SH2 DOMAIN

Experiment	References
Sequential resonance assignments	
3D CBCA(CO)NH	Grzesiek and Bax (1992a)
3D CBCANH	Grzesiek and Bax 1992b)
3D HNCO	Muhandiram and Kay (1994)
3D gd-HCACO	Zhang and Gmeiner (1996a)
3D HCA(CO)N	Powers et al. (1991)
Side-chain resonance assignments	
3D HBHA(CO)NH	Grzesiek and Bax (1993a)
3D C(CO)NH	Grzesiek et al. (1993)
3D H(CCO)NH	Grzesiek et al. (1993)
3D ^{15}N-edited TOCSY-HSQC	Zhang et al. (1994)
3D gd-HCACO-TOCSY	Zhang and Gmeiner (1996a)
3D HCCH-TOCSY	Kay et al. (1993)
3D HCCH-COSY	Bax et al. (1990)
2D (HB)CB(CGCD)HD	Yamazaki et al. (1993)
2D (HB)CB(CGCDCE)HE	Yamazaki et al. (1993)
3D LRCC	Bax et al. (1994)
Distance restraints	
3D ^{15}N-edited NOESY-HSQC	Zhang et al. (1994)
3D ^{13}C'-edited NOESY-H(N)CO	Zhang et al. (1996)
4D CN-NOESY	Muhandiram et al. (1993)
4D NN-NOESY	Ikura et al. (1990)
3D NOESY-(HCACO)NH	Zhang and Gmeiner (1996b)
4D CC-NOESY	Vuister et al. (1993)
Torsion angle restraints	
2D HMQC-J	Kay and Bax (1990)
3D HNHA	Figure 1A
3D HN(CO)CO	Hu and Bax (1996)
3D HNHB	Archer et al. (1991)
3D HN(CO)HB	Grzesiek et al. (1992)
3D HACAHB-COSY	Figure 1B
3D LRCC	Bax et al. (1994)
Proton exchange rates	
2D HSQC exchange	Grzesiek and Bax (1993b)

fected macrophages (Briggs et al., 1997). Hck is also activated in myelogenous cells that express Bcr-Abl, the gene product of the Philadelphia chromosomal rearrangement, suggesting a role for Hck activation during chronic myelogenous leukemia (Danhauser-Riedl et al., 1996).

The kinase activity of Src-family PTKs is negatively regulated as a consequence of intramolecular interactions between the residues in the C-terminal region and the SH2 domain. Negative regulation of kinase activity is dependent on the phosphorylation status of a tyrosine residue (Tyr^{527} in c-Src, Tyr^{501} in Hck) near the C-terminus that is a substrate for the C-terminal Src kinase (Csk; Nada et al., 1991). Mutations in Src-family PTKs that inhibit intramolecular binding of the phosphorylated C-terminal region to the SH2 domain have resulted in kinases that are constitutively active and capable of transforming fibroblasts (Hunter, 1987; Hirai and Varmus, 1990). Recent studies have established a critical role for the SH3 domain in negative regulation as well (for a review, see Brown and Cooper (1996)).

Structural information is essential for a full understanding of SH2 domain function in the regulation of Hck tyrosine kinase activity. The crystal structures for the regulatory and kinase domains of c-Src and Hck have been published (Sicheri et al., 1997; Xu et al., 1997). In order to understand the structural basis for specificity and binding dynamics at the molecular level in a fully solvated system, we have solved the three-dimensional (3D) solution structure of the uncomplexed Hck SH2 domain using NMR spectroscopy.

Materials and Methods

Protein preparation

The Hck SH2 domain (residues Glu^{119}–Lys^{224} of human Hck) was expressed in *E. coli* as described previously (Zhang et al., 1997). Samples for NMR analysis were prepared in 90% H_2O/10% D_2O containing 100 mM NaCl, 5 mM DTT-d_{10}, and 50 mM sodium phosphate at pH 6.4. NMR tubes were sealed after the samples were purged with argon.

NMR spectroscopy

All pulse sequences used for the structure determination of the Hck SH2 domain are listed in Table 1. Since all NMR samples were prepared in 90% H_2O, most of the pulse sequences were modified for improving suppression of the water signal. In general, pulse sequences involving the detection of amide protons were modified to incorporate the WATERGATE element (Piotto et al., 1992), while ZZ-/Z-filters (Wider and Wüthrich, 1993) were added to pulse sequences involving the detection of protons attached to carbon. The incorporation of these modifications into the HNHA and the HACAHB-COSY experiments is shown in Fig. 1. The heteronuclear (^{15}N or ^{13}C) 180° pulse following the t_2 evolution period is employed to separate the magnetization of interest from that of water, so that they have different phases at the end of the refocusing period (δ'). For the HNHA experiment (Fig. 2A), the magnetization of water is flipped back to +z prior to the WATERGATE element (Fig. 1A). In the case of the HACAHB-COSY experiment (Fig. 2B), however, the magnetization of interest is stored in z while the magnetization of water in the xy plane is dephased by the gradient pulse g4. The coupling constant, J ($^3J[H^N\text{-}H^\alpha]$ or $^3J[H^\alpha\text{-}H^\beta]$), is related to the intensities of the cross peak (I_C) and the diagonal peak (I_D) (Vuister and Bax, 1993; Grzesiek et al., 1995).

$$I_C/I_D = -\tan(2\pi J\delta)\tan(2\pi J\delta') \approx -\tan^2[\pi J(\delta+\delta')] \quad (1)$$

All NMR data were collected at 28 °C using a Varian Unity 500 spectrometer equipped with a triple-resonance probe and pulsed-field gradient accessories. NMR data were processed using either Felix v. 2.05 (Hare Research Inc., Bothel, WA) or NMRPipe (Delaglio et al., 1995) on a Sparc-20 workstation.

Sequence-specific resonance assignments

Sequential resonance assignments for the Hck SH2 domain were made using the CBCA(CO)NH (Grzesiek and Bax, 1992a) and CBCANH (Grzesiek and Bax, 1992b) experiments. Sequential $^{13}C'$ resonances were assigned using the HNCO experiment (Muhandiram and Kay, 1994). Sequential gaps due to proline residues were connected using the gd-HCACO (Zhang and Gmeiner, 1996a) and HCA(CO)N (Powers et al., 1991) experiments. These two experiments were also used to resolve ambiguities due to resonance overlap in the CBCA(CO)NH and CBCANH spectra. Side-chain resonance assignments were performed using HBHA(CO)NH (Grzesiek and Bax, 1993a), C(CO)NH, H(CCO)NH (Grzesiek et al., 1993), ^{15}N-edited TOCSY-HSQC (Zhang et al., 1994), gd-HCACO-TOCSY (Zhang and Gmeiner, 1996a), HCCH-TOCSY (Kay et al., 1993), HCCH-COSY (Bax et al., 1990), (HB)CB(CGCD)HD, and (HB)CB(CGCDCE)HE (Yamazaki et al., 1993) experiments. Methionine ε-methyl groups were assigned using the LRCC experiment (Bax et al., 1994). The ^{1}H, ^{15}N, and ^{13}C resonance assignments for the Hck SH2 domain are included as supplementary material.

Torsion angle restraints

The homonuclear three-bond coupling constant, $^{3}J[H^{N}\text{-}H^{\alpha}]$, was determined using HNHA (Fig. 1A) and HMQC-J (Kay and Bax, 1990) experiments. $^{3}J[H^{N}\text{-}H^{\alpha}]$ was used to derive ϕ torsion angle restraints based on the Karplus relationship (Wüthrich, 1986). Restraints for the ϕ torsion angle were set to $-120 \pm 30°$ (for $^{3}J[H^{N}\text{-}H^{\alpha}] > 9$ Hz), $-120 \pm 50°$ (for 8 Hz $< {}^{3}J[H^{N}\text{-}H^{\alpha}] < 9$ Hz), or $-60 \pm 30°$ (in the α-helix region only if $^{3}J[H^{N}\text{-}H^{\alpha}] < 6$ Hz). Values for the three-bond coupling constant, $^{3}J[C'\text{-}C']$, were obtained using the HN(CO)CO experiment (Hu and Bax, 1996). $^{3}J[C'\text{-}C']$ was also used to derive restraints for the ϕ torsion angle. For example, ϕ was restrained to $-150 \pm 30°$ (for $^{3}J[C'\text{-}C'] > 2$ Hz and $^{3}J[H^{N}\text{-}H^{\alpha}] > 7$ Hz) or $-170 \pm 50°$ (for $^{3}J[C'\text{-}C'] > 2$

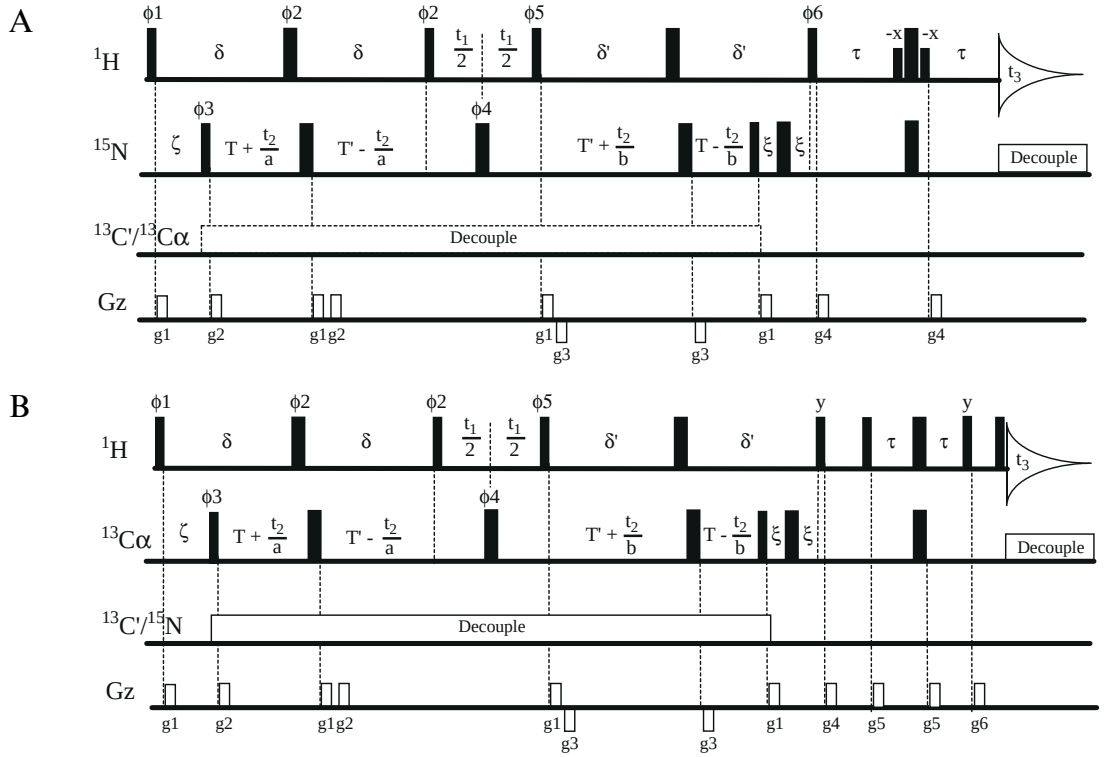

Fig. 1. Pulse schemes of (A) the HNHA experiment (Vuister and Bax, 1993) with WATERGATE (Piotto et al., 1992) and (B) the HACAHB-COSY experiment (Grzesiek et al., 1995) with ZZ-/Z-filters (Wider and Wüthrich, 1993). Narrow and wide pulses have flip angles of 90° and 180°, respectively. Unless otherwise indicated, pulses are applied along the x-axis. The phase cycle is as follows: ϕ1 = x,–x; ϕ2 = x; ϕ3 = 2(x),2(–x); ϕ4 = 4(x),4(y),4(–x),4(–y); ϕ5 = 2(x),2(–x); ϕ6 = x,–x,–x,x; receiver = x,–x,–x,x,–x,x,x,–x. Quadrature detection in t_1 and t_2 is obtained with the States-TPPI method by incrementing ϕ1 and ϕ2 for t_1 and ϕ3 for t_2. The delays employed for the HNHA experiment are: $\tau = 2.5$ ms, $T = 6.9$ ms, $T' = 12.3$ ms, while $\tau = 1.6$ ms, $T = 5.25$ ms, $T' = 8.75$ ms are used for the HACAHB-COSY experiment. Additional delays are: $\delta = T' + 2pw90^{X}$; $\delta' = T' - 2pw90^{H}$; $\zeta = \delta + 2pw90^{H} - T - pw90^{X}$; $\xi = (\delta' - T - 3pw90^{X})/2 - pw90^{X}$, where $pw90^{H}$ and $pw90^{X}$ are the 90° pulse durations for ^{1}H and ^{15}N (or ^{13}C), respectively. The values of a and b are $2(T + T')/T'$ and $2(T + T')/T$, respectively. The gradient pulses (rectangular) have different strengths and durations for each gradient. Carbon decoupling in the HNHA experiment is omitted for samples labeled with ^{15}N only. Strip plots of the HNHA and HACAHB-COSY spectra of the Hck SH2 domain in H_2O are shown in Fig. 2.

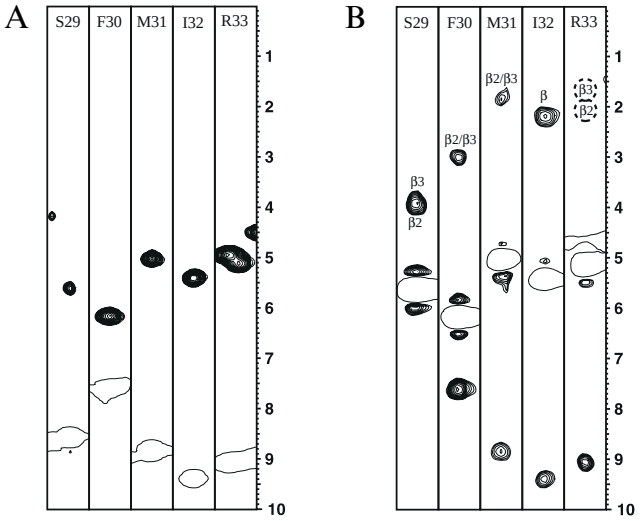

Fig. 2. (A) F1 strips from the 3D HNHA spectrum of the Hck SH2 domain. The spectrum resulted from a $64 \times 32 \times 512$ complex data matrix with spectrum widths of 6000 Hz (t_1), 1500 Hz (t_2), and 6000 Hz (t_3). The number of scans for each fid was 8 and the total measuring time was 20 h. The data were apodized in t_1 by a cosine-squared bell. In the t_2 dimension, the number of data points was doubled by mirror image linear prediction prior to cosine-squared bell apodization. The digital resolution of the final 3D spectrum was 23.4 Hz (F1), 11.7 Hz (F2), and 11.7 Hz (F3). Positive peaks were drawn with one contour level. (B) F1 strips from the 3D HACAHB-COSY spectrum of the Hck SH2 domain. The spectrum resulted from a $40 \times 48 \times 512$ complex data matrix with spectrum widths of 6000 Hz (t_1), 3000 Hz (t_2), and 6000 Hz (t_3). The number of scans for each fid was 16 and the total measuring time was 36 h. The data were apodized in t_1 by a 70°-shifted squared sine bell. In the t_2 dimension, the number of data points was doubled by mirror image linear prediction prior to cosine-squared bell apodization. The digital resolution of the final 3D spectrum was 23.4 Hz (F1), 11.7 Hz) (F2), and 11.7 Hz (F3). Positive peaks were drawn with one contour level.

Hz and $^3J[H^N\text{-}H^\alpha] < 7$ Hz). Stereospecific resonance assignments of β-methylene resonances and determination of χ^1 torsion angle restraints were performed using the HNHB (Archer et al., 1991), HN(CO)HB (Grzesiek et al., 1992), and HACAHB-COSY (Fig. 1B) experiments. For cases where the coupling constant data indicated the predominance of one rotamer (60°, –60°, or 180°) and were consistent with NOE data, the χ^1 torsion angle was constrained within 30° of the appropriate staggered rotamer conformation. NOE information was used for the stereospecific resonance assignments of valine γ-methyl groups after χ^1 was determined. Stereospecific resonance assignments of leucine δ-methyl groups and determination of χ^2 torsion angle restraints were performed using $^3J[C^\alpha\text{-}C^\delta]$ coupling constants and NOE data (Powers et al., 1993; Bax et al., 1994).

Distance restraints

NOE distance restraints were obtained from several NOESY experiments using a mixing time of 100 ms (Table 1). The 3D ^{13}C'-edited NOESY-H(N)CO experiment (Zhang et al., 1996) was used to resolve ambiguities due to overlapped amide resonances. The 3D NOESY-(HCACO)NH experiment (Zhang and Gmeiner, 1996b) was used to detect NOEs that involve H^α for samples dissolved in H_2O. In order to establish a reference for deriving distance restraints from NOE data, 13 protein structures (mainly helix, mainly sheet, or both) from the Brookhaven Protein Databank were randomly selected for analysis. In all cases, the $H^N\text{-}H^\alpha$ distance for all 1141 non-glycine and non-proline residues correlated well with the ϕ torsion angle. Since ϕ is related to $^3J[H^N\text{-}H^\alpha]$ via the Karplus relationship (Wüthrich, 1986), the intraresidue $H^N\text{-}H^\alpha$ distance was calculated directly from $^3J[H^N\text{-}H^\alpha]$ and geometrical parameters (Fig. 3). The intraresidue $H^N\text{-}H^\alpha$ distance obtained in this manner was then used as a reference for converting other NOE intensities (NOEs between amide protons and carbon-attached protons) into distance restraints. When the $H^N\text{-}H^\alpha$ distance was used as a reference for a different residue (e.g., glycine), NOE intensities were corrected for signal loss due to relaxation (Meadows et al., 1993). Values of $^3J[H^N\text{-}H^\alpha]$ smaller than 7 Hz can be correlated with either of two possible $H^N\text{-}H^\alpha$ distances corresponding to four different ϕ torsion angles (Wüthrich, 1986). Initially, only the longer of these two distances was used as a reference in converting NOE intensities into distance restraints since the probability of the shorter $H^N\text{-}H^\alpha$ distance is much smaller than that of the longer distance (Fig. 3). The shorter $H^N\text{-}H^\alpha$ distance corresponds to a ϕ torsion angle of 60° and is characterized

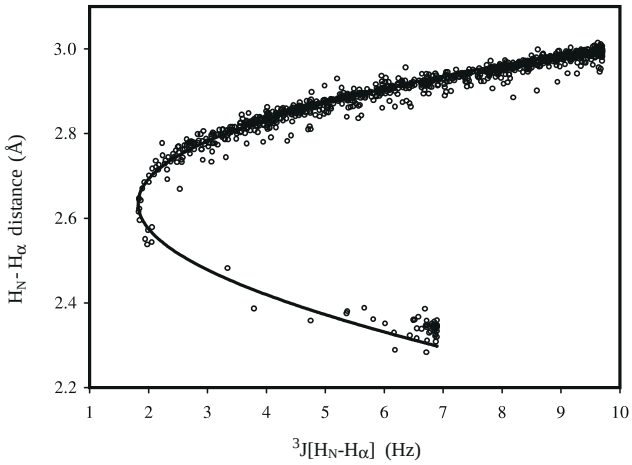

Fig. 3. Intraresidue $H^N\text{-}H^\alpha$ distance as a function of the homonuclear three-bond coupling constant, $^3J[H^N\text{-}H^\alpha]$. Circles represent measured values for 1141 amino acid residues from 13 solution structures in the Brookhaven Protein Databank (ID codes are 1BTA, 1CRE, 1BBN, 1HWA, 2PNB, 1PNJ, 2PLD, 2GB1, 1CRR, 1COO, 1HCS, 1FRC, and 1SRL). For each residue, the ϕ torsion angle and $H^N\text{-}H^\alpha$ distance were evaluated and the measured value of ϕ was converted to $^3J[H^N\text{-}H^\alpha]$ using the Karplus equation: $^3J[H^N\text{-}H^\alpha] = 6.4\cos^2(\phi - 60) - 1.4\cos(\phi - 60) + 1.9$ (Wüthrich, 1986). The solid line represents the theoretical values based on the Karplus equation and the following geometrical parameters: bond $[H^N\text{-}N] = 1.020$ Å, bond $[C^\alpha\text{-}H^\alpha] = 1.100$ Å, bond $[N\text{-}C^\alpha] = 1.458$ Å, angle $[H^N\text{-}N\text{-}C^\alpha] = 119.0°$, angle $[N\text{-}C^\alpha\text{-}H^\alpha] = 108.3°$.

by a strong intraresidue H^N-H^α NOE and large $^3J[C'\text{-}H^\alpha]$ coupling constant. When such a distance was confirmed for a residue in the initial structures, restraints were modified using the shorter H^N-H^α distance as a reference. Similarly, the intraresidue H^α-H^β distance (in Ile, Thr, and Val) is mainly related to the χ^1 torsion angle as in Table 2.

After χ^1 is determined, the intraresidue H^α-H^β distance can be used as a reference to convert NOEs between two carbon-attached protons into distance restraints. In high-resolution protein structures, the three staggered rotamer conformations of χ^1 vary in the range of $64.1 \pm 15.7°$, $183.6 \pm 16.8°$, and $-66.7 \pm 15.0°$, respectively (Laskowski et al., 1993). Therefore, the averaged NOE intensity corresponding to a particular H^α-H^β distance (either 2.5 Å or 3.0 Å) was used as a reference in this work. H^N-H^N distance restraints were obtained using the normal method (Wüthrich, 1986). The upper limits of NOE distance restraints were classified into six groups: 2.5, 3.0, 3.5, 4.2, 5.0, and 6.0 Å.

Hydrogen bonding restraints

Amide proton exchange rates were estimated using the HSQC exchange experiment (Grzesiek and Bax, 1993b). Locations of hydrogen bonds were determined based on qualitative exchange rates for amide protons and an examination of intermediate structures. Distance restraints of 1.8–2.4 Å (H^N to O) and 2.5–3.4 Å (N to O) were applied for the hydrogen bond donor–acceptor pairs identified.

TABLE 2
H^α-H^β DISTANCE RESTRAINTS FOR χ^1 ANGLES

	χ^1		
	60°	180°	−60°
H^α-H^β (Ile) (Å)	2.5	2.5	**3.0**
H^α-H^β (Thr) (Å)	**2.5**	2.5	3.0
H^α-H^β (Val) (Å)	2.5	**3.0**	2.5

Structure calculations

Solution structures for the Hck SH2 domain were calculated with DYANA v. 1.2 (Güntert et al., 1996) using simulated annealing and molecular dynamics in torsion angle space. DYANA calculates structures by adjusting torsion angles to fit conformational restraints derived from experimental data while all covalent structure parameters (bond lengths, bond angles, chiralities, and planarities) are kept at their optimal values. Initially, the temperature of the system was increased to 8.0 TFU (target function units) per residue, followed by 2000 steps of molecular dynamics (MD). The system was then slowly cooled during 10 000 MD steps to a final temperature of 0.0 TFU. Finally, structures were minimized using 1000 steps of conjugate gradient minimization. Initial structures were calculated using only unambiguous distance and torsion angle restraints while additional restraints were included during successive cycles of structural refinement. In the final cycle of calculation, 40 structures were generated and the 20 structures having the lowest target functions were selected for analysis.

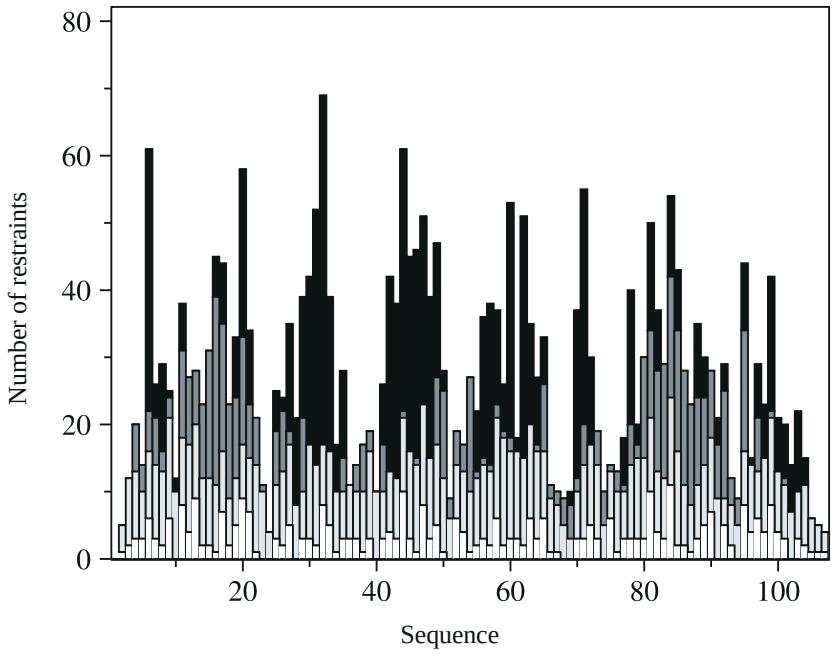

Fig. 4. Histogram showing the distribution of NMR distance restraints used in the structural calculation of the Hck SH2 domain. The primary sequence is numbered such that the N-terminal methionine from bacterial expression is residue 1 and the highly conserved tryptophan is residue 6. The bar-coded restraint categories are as follows: white, intraresidue; light gray, sequential ($|i-j|=1$); dark gray, medium-range ($2 \le |i-j| < 5$); black, long-range ($|i-j| \ge 5$).

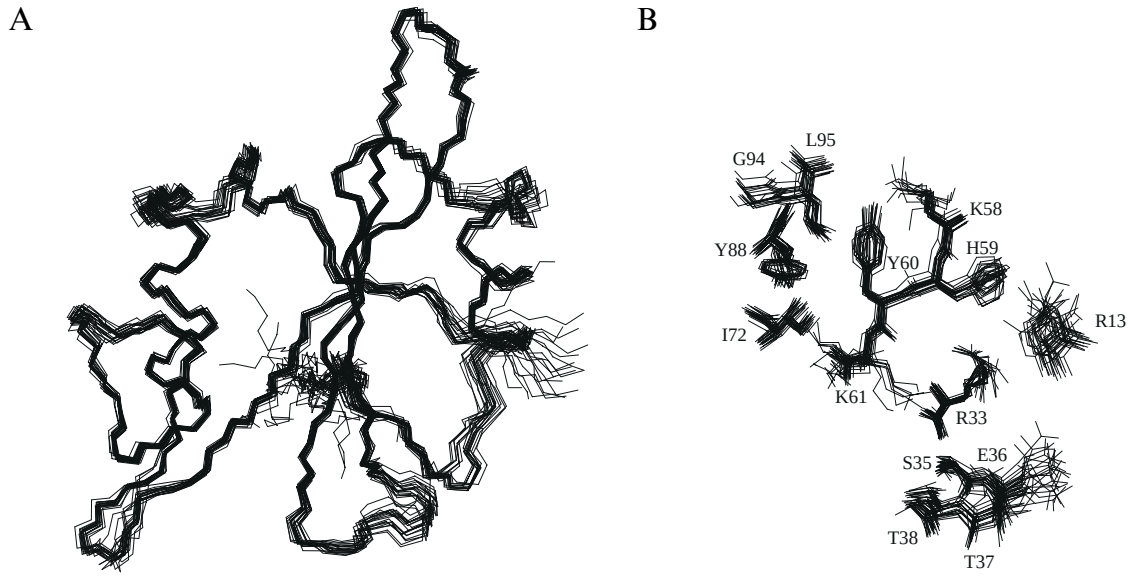

Fig. 5. Superimposed view of the 20 NMR structures of the Hck SH2 domain. (A) Best-fit superposition of the backbone (N,C^{α},C') atoms for residues 5–104. (B) All heavy atoms for those residues that are involved in ligand binding. These figures were generated using the program MOLMOL (Koradi et al., 1996).

Results

Experimental restraints

A total of 1757 significant restraints including 1580 distance restraints (78 restraints were from 39 hydrogen bond donor–acceptor pairs), 93 ϕ restraints, 72 χ^1 restraints, and 12 χ^2 restraints (8 Leu and 4 Ile) were derived from multidimensional NMR experiments. The distance restraints consisted of 355 intraresidue, 500 sequential ($|i-j|=1$), 238 medium-range ($2 \le |i-j| < 5$), and 487 long-range ($|i-j| \ge 5$). The number of distance restraints for each residue is shown in Fig. 4. Atoms that could not be assigned stereospecifically were treated as pseudoatoms during the structure calculations.

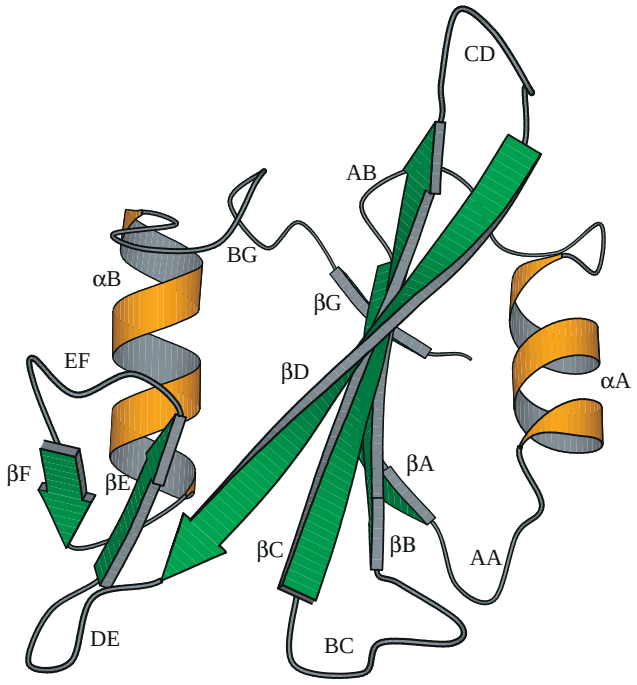

Fig. 6. Ribbon diagram showing the backbone secondary structure for the Hck SH2 domain. This figure was generated using the MOLSCRIPT program (Kraulis, 1991). The secondary structure elements were labeled according to the nomenclature of Eck et al. (1993).

Quality of the converged solution structures

The 20 structures having the lowest target functions during the final cycle of structure calculation were selected to represent the ensemble of conformations for the Hck SH2 domain in solution. A superimposed stereoview of the 20 structures is presented in Fig. 5A for backbone atoms and in Fig. 5B for residues that are involved in ligand binding. Since all covalent parameters were kept at their optimal values during structure calculation with DYANA, the target function is a measure of the number and magnitude of violations from experimental restraints as well as van der Waals clashes. All 20 structures in the ensemble satisfied the experimental restraints extremely well. The largest violation of distance restraints was 0.17 Å and the largest violation of torsion angle restraints was 0.4°. The average rmsd values between the 20 individual structures and the mean coordinates were 0.42 ± 0.08 Å for the N,C^{α},C' atoms and 0.81 ± 0.08 Å for all heavy atoms (residues 5–104). Limiting the comparison to those residues in regions of ordered secondary structure resulted in rmsd values of 0.27 ± 0.04 Å for the N,C^{α},C' atoms and 0.73 ± 0.06 Å for all heavy atoms. A Ramachandran plot of the backbone ϕ and ψ torsion angles for the 20 structures revealed that 81.1% of the residues lie in the most favored regions according to PROCHECK (Laskowski et

```
      1       10        20        30        40        50        60        70        80        90       100
      +........+.........+.........+.........+.........+.........+.........+.........+.........+.........+.....
Hck   METEEWFFKGISRKDAERQLLAPGNMLGSFMIRDSETTKGSYSLSVRDYDPRQGDTVKHYKIRTLDNGGFYISPRSTFSTLQELVDHYKKGNDGLCQKLSVPCMSSK

c-Src IQAEEWYFGKITRRESERLLLNAENPRGTFLVRESETTKGAYCLSVSDFDNAKGLNVKHYKIRKLDSGGFYITSRTQFNSLQQLVAYYSKHADGLCHRLTTVCP

Lck   LEPEPWFFKNLSRKDAERQLLAPGNTHGSFLIRESESTAGSFSLSVRDFDQNQGEVVKHYKIRNLDNGGFYISPRITFPGLHELVRHYTNASDGLCTRLSRPCOT

Blk   LEVEKWFFRTISRKDAERQLLAPMNKAGSFLIRESESNKGAFSLSVKDIT-TQGEVVKHYKIRSLDNGGYYISPRITFPTLQALVQHYSKKGDGLCQKLTLPCVNLA
            βA        αA              βB              βC              βD        βE    βF        αB              βG
```

Fig. 7. Sequence alignment for the SH2 domains from Src-family PTKs whose structures have been solved using either X-ray crystallography or NMR spectroscopy. Underlined residues have been determined to be in the ordered regions of secondary structure. The second line under the Hck SH2 sequence represents the secondary structure elements reported in the crystal structure of Hck (Sicheri et al., 1997).

al., 1993). Only two residues (0.1%) were in the disallowed regions and these were near the termini of the domain (data not shown). The coordinates of the 20 solution structures have been deposited in the Brookhaven Protein Databank. The ID code is 3hck.

Conformation of the solution structures

A ribbon diagram depicting the solution structure of the Hck SH2 domain is presented in Fig. 6. The overall conformation of the Hck SH2 domain in solution is similar to SH2 domains from other Src-family PTKs. It consists of seven β-strands and two α-helices. Three strands form the central β-sheets (βB, βC, βD) which are flanked by two α-helices (αA, αB). Residues included in the ordered regions of secondary structure are Trp^{6}–Phe^{8} (βA), Arg^{13}–Leu^{21} (αA), Ser^{29}–Asp^{34} (βB), Ser^{41}–Tyr^{49} (βC), Asp^{55}–Thr^{64} (βD and βD'), Gly^{69}–Ile^{72} (βE), Thr^{77}–Ser^{79} (βF), Leu^{81}–Gly^{91} (αB), and Val^{101}–Cys^{103} (βG). The alignment of the primary sequence and secondary structure of the Hck SH2 domain with SH2 domains from three other Src-family PTKs is shown in Fig. 7 (Xu et al., 1995; Metzler et al., 1996; Tong et al., 1996; Sicheri et al., 1997).

Comparisons between the solution structure of the Hck SH2 domain with the SH2 domain from the crystal structures of the regulatory and kinase domains of Hck are shown in Fig. 8 (Sicheri et al., 1997). The crystal structure of the uncomplexed v-Src SH2 domain is also included in Fig. 8 for comparison. Superimposition of backbone (n,C^{α},C') atoms in the mean solution structure (residues 5–104) upon the SH2 domains from the crystal structures of Hck/AMP-PNP and Hck/quercetin complexes yielded rmsd values of 1.38 Å and 1.35 Å, respectively. Large

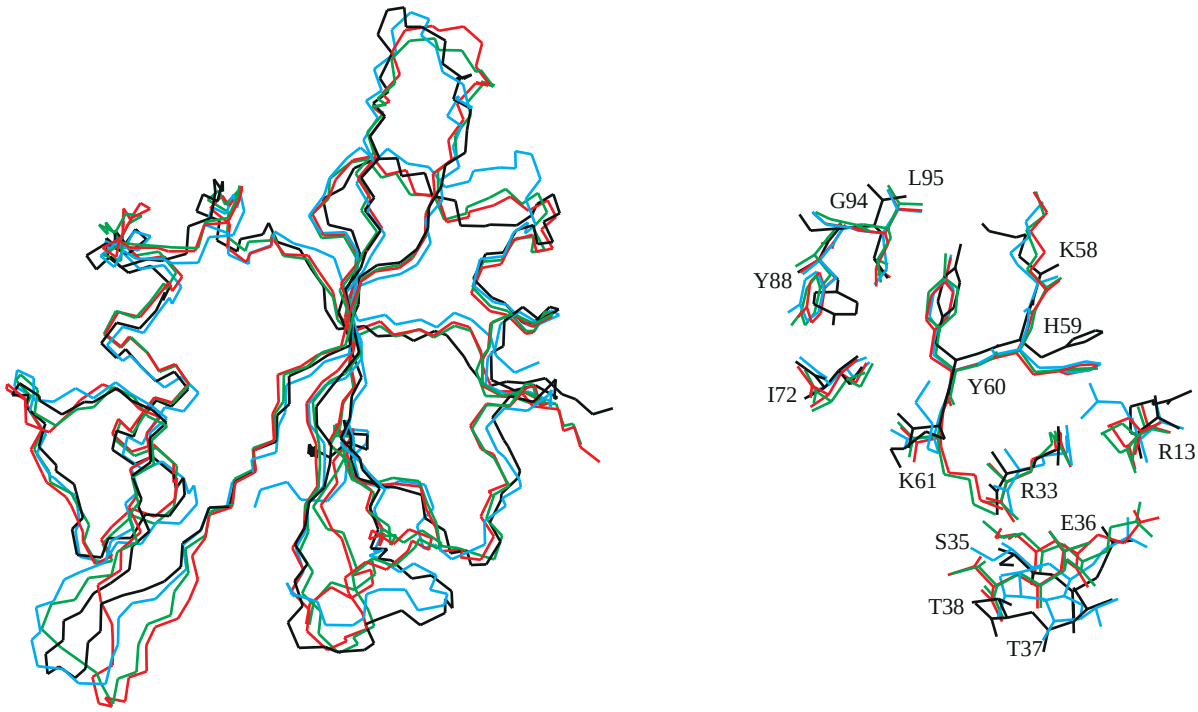

Fig. 8. Comparison of (A) backbone and (B) ligand binding region of the solution structure of the Hck SH2 domain (black) with the SH2 domain from the crystal structure of Hck in complex with AMP-PNP (red) and Hck in complex with quercetin (green) (Sicheri et al., 1997), and the crystal structure of the uncomplexed v-Src SH2 domain (light blue) (Waksman et al., 1993).

deviations were limited to the loop regions. Restricting the comparison to residues in ordered regions of secondary structure resulted in rmsd values of 0.85 Å and 0.82 Å, respectively. Deviations in the BC and EF loop regions are probably the result of ligand binding in the X-ray structures (Waksman et al., 1993). Titration of the Hck SH2 domain with a high-affinity peptide also showed a large change in chemical shifts of the amide resonances for residues in these loop regions (data not shown). In the DE loop, two conformations have been identified, a result similar to that reported for the solution structure of the Blk SH2 domain (Metzler et al., 1996). The major differences between the two conformations are residues Gly^{68} and Gly^{69} which have different ϕ and ψ torsion angles in the two conformations. Interestingly, the SH2 domain from the two crystal structures of Hck also has large differences in this region, suggesting that the DE loop is flexible (Fig. 8A).

The mean solution structure of the Hck SH2 domain is also similar to the crystal structure of the uncomplexed v-Src SH2 domain (Waksman et al., 1993). Superimposition of the backbone (N,C^{α},C') atoms for these two structures gave an rmsd of 1.82 Å (residues 5–104). Restricting the comparison to ordered regions of secondary structure resulted in an rmsd of 0.87 Å. The conformation of side chains for residues involved in ligand binding in the structures solved using X-ray crystallography is also similar to the conformation for these side chains in the solution structure (Fig. 8B). Large deviations in side-chain conformation between the solution structure of the uncomplexed Hck SH2 domain and the Hck SH2 domain from the crystal structure of Hck are observed for Arg^{13} and residues located in the BC loop (Ser^{35}–Thr^{38}).

Discussion and Conclusions

H^N-H^{α} distance as a reference

The precision and accuracy of molecular structures determined using NMR spectroscopic data are limited by the number of distance and torsion angle restraints and also by the precision and accuracy of each individual restraint (Clore and Gronenborn, 1993). Torsion angle restraints are normally derived from scalar coupling constants using the Karplus relationship. For distance restraints, however, a reference is needed in order to convert NOE intensities into distance restraints. The backbone interproton distances in regular secondary structure elements (Wüthrich, 1986) have been commonly used as references. The disadvantage of this practice is that a secondary structure element has to be identified before converting NOE intensities into distance restraints. In order to find a simple distance reference, we have analyzed the intraresidue H^N-H^{α} distance and found that the H^N-H^{α} distance is highly correlated with ϕ for protein structures deposited in the Brookhaven Protein Databank. Estimation of the H^N-H^{α} distance from geometrical parameters and the scalar coupling constant, $^3J[H^N$-$H^{\alpha}]$, is therefore a straightforward exercise. The distance obtained in this manner can be used as a reference to convert other NOE intensities into distance restraints. In this manner, attenuation of NOE intensities due to amide proton exchange is, to a first approximation, accounted for in the estimation of distances between the amide proton and carbon-attached protons. Our solution structures for the Hck SH2 domain were determined using distance constraints determined in this manner, and these structures closely resemble those for other SH2 structures solved using either NMR spectroscopy or X-ray crystallography.

Comparison of NMR and X-ray structures

Recently, a major breakthrough in the structural biology of Src-family PTKs was achieved with the elucidation of the 3D structures for the regulatory and kinase domains of c-Src and Hck that were each solved using X-ray crystallography (Sicheri et al., 1997; Xu et al., 1997). These structures indicate that negative regulation of kinase activity in Src-family PTKs probably arises from simultaneous interaction of the SH3 domain with the SH2-kinase linker concomitant with the binding of the SH2 domain to the phosphotyrosine near the C-terminus of the kinase. These interactions, which occur on the opposite side of the kinase domain from the active site, serve to regulate the relative orientation of the two lobes of the kinase domain and thus to modulate kinase activity.

The X-ray structures reported for the regulatory and kinase domains of Hck and c-Src do little to dispel the notion that the regulatory domains of Src-family PTKs are essentially modular in their structural and ligand binding properties. The overall topology of our solution structure for the Hck SH2 domain does not differ substantially from the SH2 domains in either of the X-ray structures reported for Hck (Fig. 8). Despite the overall similarity between our NMR structures and the X-ray structures of the Hck SH2 domain, several notable differences were observed. These differences were, for the most part, localized in the loop regions that connect ordered secondary structure elements. Rmsd values for all residues not involved in loop regions were less than 0.9 Å. Backbone rmsd values for the 20 NMR structures were only moderately larger for residues in these loop regions, demonstrating that the structures were well constrained by the spectroscopic data. Proton exchange rates indicated that amide protons in the loop regions were solvent accessible and ^{15}N relaxation data indicated that some residues in the loop regions have small order parameters (data not shown), indicating that these regions are more flexible than that of the ordered secondary structure elements. Another possibility for the conformational differences in the loop regions between the structures determined using X-ray crystallography and NMR spectroscopy is crystal

packing forces. Differences in the conformation for these loop regions were also apparent in a comparison between the solution structure of the uncomplexed Hck SH2 domain with the crystal structure of the uncomplexed v-Src SH2 domain (Waksman et al., 1993).

Biological relevance

Gene-knockout experiments have demonstrated redundancy in Src-family PTK function, yet nature has selected nine members of the Src-family PTKs as being required for the optimal function of multicellular organisms. Our studies of the solution structure for the SH2 domain from the Src-family PTK, Hck, revealed that while the same structural principles dictate the function of this SH2 domain as is the case for other SH2 domains, subtle differences in the conformation for residues that line the binding pocket are probably responsible for the unique binding specificity. Binding of the phosphorylated tail region to SH2 domains is normally a weak interaction as is the recognition of SH3 domains by the SH2-kinase linker region as revealed in the crystal structure of Hck (Sicheri et al., 1997). Activation of Src-family PTKs thus requires the displacement of two low-affinity binding events. The structural data presented here are useful for further studying the binding specificity and dynamics of the Hck SH2 domain at the molecular level in a fully solvated system. This will provide valuable information for the modeling and design of new inhibitor candidates.

Acknowledgements

We thank David Babcook for NMR instrumental assistance. This research was supported in part by grants from the National Institutes of Health (NIH-NCI CA-36727, NIH-NCI CA58667 (T.E.S.)), the American Cancer Society (IRG-165G (W.H.G.)) and the Nebraska Department of Health (W.H.G.).

References

Archer, S.J., Ikura, M., Torchia, D.A. and Bax, A. (1991) *J. Magn. Reson.*, **95**, 636–641.

Bax, A., Clore, G.M., Driscoll, P.C., Gronenborn, A.M., Ikura, M. and Kay, L.E. (1990) *J. Magn. Reson.*, **87**, 620–627.

Bax, A., Delaglio, F., Grzesiek, S. and Vuister, G.W. (1994) *J. Biomol. NMR*, **4**, 787–797.

Bohuslav, J., Horejsi, V., Hansmann, C., Stockl, J., Weidle, U.H., Majdic, O., Bartke, I., Knapp, W. and Stockinger, H. (1995) *J. Exp. Med.*, **181**, 1381–1390.

Boulet, I., Ralph, S., Stanley, E., Lock, P., Dunn, A.R., Green, S.P. and Phillips, W.A. (1992) *Oncogene*, **7**, 703–710.

Briggs, S.D., Sharkey, M., Stevenson, M. and Smithgall, T.E. (1997) *J. Biol. Chem.*, **272**, 17899–17902.

Brown, M.T. and Cooper, J.A. (1996) *Biochim. Biophys. Acta*, **1287**, 121–149.

Clore, G.M. and Gronenborn, A.M. (1993) In *NMR of Proteins* (Eds., Clore, G.M. and Gronenborn, A.M.), CRC Press, Boca Raton, FL, U.S.A., pp. 1–32.

Danhauser-Riedl, S., Warmuth, M., Druker, B.J., Emmerich, B. and Hallek, M. (1996) *Cancer Res.*, **56**, 3589–3596.

Delaglio, F., Grzesiek, S., Vuister, G.W., Zhu, G., Pfeifer, J. and Bax, A. (1995) *J. Biomol. NMR*, **6**, 277–293.

Durden, D.L., Kim, H.M., Calore, B. and Liu, Y. (1995) *J. Immunol.*, **154**, 4039–4047.

Eck, M.J., Atwell, S.K., Shoelson, S.E. and Harrison, S.C. (1993) *Nature*, **368**, 764–769.

Ghazizadeh, S., Bolen, J.B. and Fleit, H.B. (1994) *J. Biol. Chem.*, **269**, 8878–8884.

Grzesiek, S. and Bax, A. (1992a) *J. Am. Chem. Soc.*, **114**, 6291–6293.

Grzesiek, S. and Bax, A. (1992b) *J. Magn. Reson.*, **99**, 201–207.

Grzesiek, S., Ikura, M., Clore, G.M., Gronenborn, A.M. and Bax, A. (1992) *J. Magn. Reson.*, **96**, 215–221.

Grzesiek, S., Anglister, J. and Bax, A. (1993) *J. Magn. Reson.*, **B101**, 114–119.

Grzesiek, S. and Bax, A. (1993a) *J. Biomol. NMR*, **3**, 185–204.

Grzesiek, S. and Bax, A. (1993b) *J. Biomol. NMR*, **3**, 627–638.

Grzesiek, S., Kuboniwa, H., Hinck, A.P. and Bax, A. (1995) *J. Am. Chem. Soc.*, **117**, 5312–5315.

Güntert, P., Mumenthaler, C. and Wüthrich, K. (1996) XVIIth International Conference on Magnetic Resonance in Biological Systems, Keystone, CO, U.S.A., August 18–23, 1996, p. 175.

Hirai, H. and Varmus, H. (1990) *Mol. Cell. Biol.*, **10**, 1307–1318.

Holtzman, D.A., Cook, W.D. and Dunn, A.R. (1987) *Proc. Natl. Acad. Sci. USA*, **84**, 8325–8329.

Hu, J.-S. and Bax, A. (1996) *J. Am. Chem. Soc.*, **118**, 8170–8171.

Hunter, T. (1987) *Cell*, **49**, 1–4.

Ikura, M., Bax, A., Clore, G.M. and Gronenborn, A.M. (1990) *J. Am. Chem. Soc.*, **112**, 9020–9022.

Kay, L.E. and Bax, A. (1990) *J. Magn. Reson.*, **86**, 110–126.

Kay, L.E., Xu, G.Y., Singer, A.U., Muhandiram, D.R. and Forman-Kay, J.D. (1993) *J. Magn. Reson.*, **B101**, 333–337.

Kestler III, H.W., Ringler, D.J., Mori, K., Panicali, D.L., Sehgal, P.K., Daniel, M.D. and Desrosiers, R.C. (1991) *Cell*, **65**, 651–662.

Klemsz, M.J., McKercher, S.R. and Maki, R.A. (1987) *Nucleic Acids Res.*, **15**, 9600–9602.

Koradi, R., Billeter, M. and Wüthrich, K. (1996) *J. Mol. Graph.*, **14**, 51–55.

Kraulis, P.J. (1991) *J. Appl. Crystallogr.*, **24**, 946–950.

Laskowski, R.A., MacArthur, M.W., Moss, D.S. and Thornton, J.M. (1993) *J. Appl. Crystallogr.*, **26**, 283–291.

Lichtenberg, U., Quintrell, N. and Bishop, J.M. (1992) *Oncogene*, **7**, 849–858.

Meadows, R.P., Nettesheim, D.G., Xu, R.X., Olejniczak, E.T., Petros, A.M., Holzman, T.F., Severin, J., Gubbins, E., Smith, H. and Fesik, S.W. (1993) *Biochemistry*, **32**, 754–765.

Metzler, W.J., Leiting, B., Pryor, K., Mueller, L. and Farmer II, B.T. (1996) *Biochemistry*, **35**, 6201–6211.

Möhn, H., Le Cabec, V., Fischer, S. and Maridonneau-Parini, I. (1995) *Biochem. J.*, **309**, 657–665.

Muhandiram, D.R., Xu, G.Y. and Kay, L.E. (1993) *J. Biomol. NMR*, **3**, 463–470.

Muhandiram, D.R. and Kay, L.E. (1994) *J. Magn. Reson.*, **B103**, 203–216.

Nada, S., Okada, M., MacAuley, A., Cooper, J.A. and Nakagawa, H. (1991) *Nature*, **351**, 69–72.

Piotto, M., Saudek, V. and Sklenář, V. (1992) *J. Biomol. NMR*, **2**, 661–665.

Powers, R., Gronenborn, A.M., Clore, G.M. and Bax, A. (1991) *J. Magn. Reson.*, **94**, 209–213.

Powers, R., Garrett, D.S., March, C.J., Frieden, E.A., Gronenborn, A.M. and Clore, G.M. (1993) *Biochemistry*, **32**, 6744–6762.

Quintrell, N., Lebo, R., Varmus, H., Bishop, J.M., Pettenati, M.J., Le Beau, M.M. and Diaz, M.O. (1987) *Mol. Cell. Biol.*, **7**, 2267–2275.

Sicheri, F., Moarefi, I. and Kuriyan, J. (1997) *Nature*, **385**, 602–609.
Tong, L., Warren, T.C., King, J., Betageri, R., Rose, J. and Jakes, S. (1996) *J. Mol. Biol.*, **256**, 601–610.
Vuister, G.W. and Bax, A. (1993) *J. Am. Chem. Soc.*, **115**, 7772–7777.
Vuister, G.W., Clore, G.M., Gronenborn, A.M., Powers, R., Garrett, D.S., Tschudin, R. and Bax, A. (1993) *J. Magn. Reson.*, **B101**, 210–213.
Waksman, G., Shoelson, S.E., Pant, N., Cowburn, D. and Kuriyan, J. (1993) *Cell*, **72**, 779–790.
Wang, A.V.T., Scholl, P.R. and Geha, R.S. (1994) *J. Exp. Med.*, **180**, 1165–1170.
Wider, G. and Wüthrich, K. (1993) *J. Magn. Reson.*, **B102**, 239–241.
Wüthrich, K. (1986) *NMR of Proteins and Nucleic Acids*, Wiley, New York, NY, U.S.A.
Xu, R.X., Word, J.M., Davis, D.G., Rink, M.J., Willard Jr., D.H. and Gampe Jr., R.T. (1995) *Biochemistry*, **34**, 2107–2121.
Xu, W., Harrison, S.C. and Eck, M.J. (1997) *Nature*, **385**, 595–602.
Yamazaki, T., Forman-Kay, J.D. and Kay, L.E. (1993) *J. Am. Chem. Soc.*, **115**, 11054–11055.
Zhang, O., Kay, L.E., Olivier, J.P. and Forman-Kay, J.D. (1994) *J. Biomol. NMR*, **4**, 845–858.
Zhang, W. and Gmeiner, W.H. (1996a) *J. Biomol. NMR*, **7**, 247–250.
Zhang, W. and Gmeiner, W.H. (1996b) *J. Biomol. NMR*, **8**, 357–359.
Zhang, W., Smithgall, T.E. and Gmeiner, W.H. (1996) *J. Magn. Reson.*, **B111**, 305–309.
Zhang, W., Smithgall, T.E. and Gmeiner, W.H. (1997) *FEBS Lett.*, **406**, 131–135.
Ziegler, S.F., Marth, J.D., Lewis, D.B. and Perlmutter, R.M. (1987) *Mol. Cell. Biol.*, **7**, 2276–2285.